

NINETEENTH EUROPEAN ROTORCRAFT FORUM

Paper n° C6

**AN IN-FLIGHT INVESTIGATION OF LYNX AH MK5
MAIN ROTOR/TAIL ROTOR INTERACTIONS.**

by

Lieutenant Commander A D S ELLIN BSc PhD Royal Navy
Defence Research Agency
Bedford, England

September 14-16, 1993
CERNOBBIO (Como)
ITALY

**ASSOCIAZIONE INDUSTRIE AEROSPAZIALI
ASSOCIAZIONE ITALIANA DI AERONAUTICA ED ASTRONAUTICA**

AN IN-FLIGHT INVESTIGATION OF LYNX AH MK5 MAIN ROTOR/TAIL ROTOR INTERACTIONS.

Lieutenant Commander A D S ELLIN BSc
Defence Research Agency,
Bedford, England.

Summary.

The analysis of pressure data collected on the DRA Research Lynx AH Mk5 tail rotor in flight has revealed that the aircraft low speed flight envelope can be divided into six regions, each with a different mechanism of main rotor/tail rotor interaction. This paper presents, in detail, mechanisms to explain the three most significant interactions and discusses, in broader terms, the remainder. The modelling of these effects to improve the fidelity of ground based flight simulation is also covered.

Notation.

ASE	Auto Stabilisation Equipment
a	lift curve slope
C_p	pressure coefficient $= \frac{P-P_0}{\frac{1}{2}\rho V^2}$
c	tail rotor blade chord
IGE	In Ground Effect
L	lift on tail rotor blade element dr
nR	"n"th harmonic of main rotor rotational frequency
nT	"n"th harmonic of tail rotor rotational frequency
OGE	Outside Ground Effect
p	pressure recorded at sensor
P_0	static pressure
R_t	tail rotor blade radius
r	distance of element dr along tail rotor blade non-dimensionalised by R_t
V	chordwise velocity at element dr
V_a	aircraft translational velocity
V_r	blade in plane velocity at radial station r induced by blade rotation and aircraft translation $\Omega_t r + V_a \sin \psi$
V_v	in-plane component of velocity induced at tail rotor blade element dr by main rotor tip vortex
α	tail rotor blade local incidence
λ	tail rotor downwash velocity non-dimensionalised by $\Omega_t R_t$
ρ	air density

θ	tail rotor blade root pitch angle
ψ	tail rotor blade azimuth angle measured from horizontally backwards in the direction of rotation
Ω_t	tail rotor rotational speed

1. Introduction.

The characteristics of the helicopter models used for flight simulation typically fail to replicate the major non-linearities evident in helicopter yaw handling and control in low speed flight. The unrepresentative symmetrical yaw pedal margin plot generated using the DRA Helistab program, as described by Padfield(1), compared with the very unsymmetric margin observed during flight trials with the Lynx AH Mk5 (figures 1 & 2), demonstrates the magnitude of the problem.

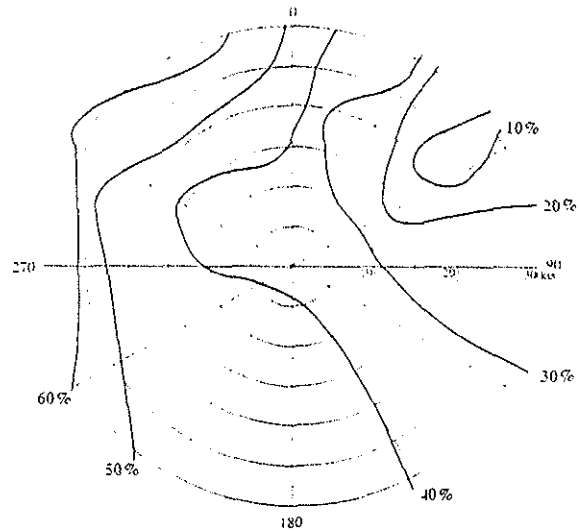


Figure 1. Plot showing the variation in yaw control margin for changes in relative wind speed and direction for the Lynx AH Mk5 recorded during the flight trial. Aircraft all up mass is 4700kg.

This failing is not unique to Helistab and, in the main, is due to a universal lack of understanding of the many interactional mechanisms that affect helicopter tail rotor performance. Consequently,

there is a dearth of information on how to model the effects of these interactions on the simulator.

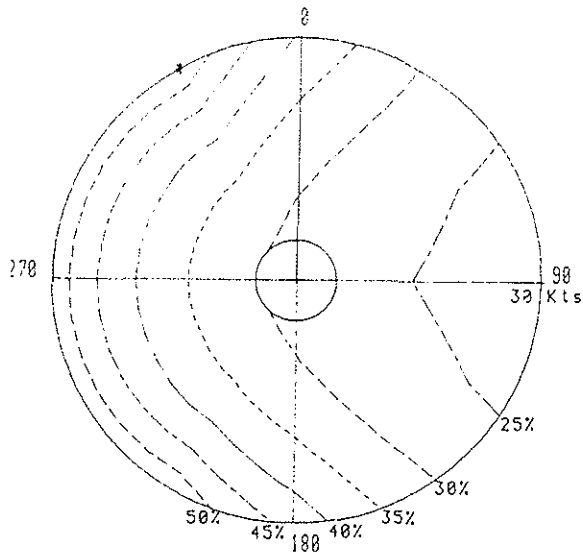


Figure 2. Plot showing the variation in yaw control margin for changes in relative wind speed and direction as calculated by Helistab when configured as a Lynx AH Mk5.

Those non-linearities are most strongly observed during nap of the earth (NOE) flying and operation to the deck of a ship where handling deficiencies cause significant problems. One of the aims of the DRA tail rotor strategic research programme carried out at Bedford was therefore to provide data that would lead to an improved understanding of these mechanisms. The factors affecting tail rotor performance could then be modelled in a manner compatible with the constraints of real time simulation.

Two flight trials have been carried out, one with a Puma⁽²⁾, the other with a Lynx AH Mk5⁽³⁾. Some of the flight events on the earlier Puma trial have been analysed^(4&5) and techniques for handling the vast quantities of data developed. This paper represents the outcome of the initial analysis of the Lynx data and discusses, in some detail, mechanisms to explain the features observed and some attempts at modelling their effects. Section 2 outlines the analysis techniques employed, after which, in section 3, mechanisms are described for some of the interactions located. The paper ends with conclusions and recommendations for further work in the field.

2. The data analysis.

The instrumented tail rotor designed and manufactured for the Lynx AH Mk5 was fitted with arrays of

leading edge and trailing edge pressure sensors for use with the pressure indicator sensor method of blade loading estimation. This method has been successfully employed by the DRA for main rotor research and has been fully described by Brotherhood and Riley⁽⁶⁾ and Brotherhood⁽⁷⁾. The design and manufacture of the blade and the subsequent conduct of the flight trial has already been reported on by Ellin⁽³⁾.

The bulk of the data analysed to date has been that recorded in the hover and during constant velocity sidestep manoeuvres. Approximately 300 of the 1270 test conditions recorded have so far been inspected. The data has proved to be of a contemporary high quality, free from excessive drop-outs and noise, easily justifying the time taken in setting up the instrumentation prior to the trial.

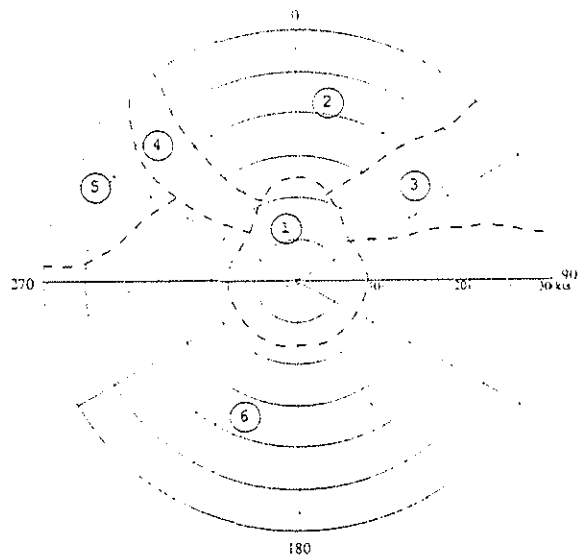


Figure 3. Lynx AH Mk5 low speed flight envelope showing regions where different main rotor tail rotor interactions were observed. Areas 3 & 4 have similar mechanisms.

Even in a steady flight condition, the tail rotor flow field varies from revolution to revolution. In order to develop a detailed understanding of the factors affecting the tail rotor it is therefore necessary to analyse the data from many revolutions for each test condition. With so much data to study, a semi-automated analysis routine was created to produce a standard set of 7 plots from each test case, summarising the information contained therein. These plots did not contain sufficient information for the interaction mechanisms to be determined, but allowed the low speed flight envelope to be divided up into regions where similar features in the data had been noted (figure 3). Once this base line analysis process

was complete, one or more events from each region of the envelope were subsequently selected for a more detailed, in-depth analysis. The aim of this two-tier analysis process was to provide the most efficient process whereby a large proportion of the data collected could be examined and the nuggets of information contained within it extracted.

Both frequency and time domain techniques were employed. Study of the signal from each leading edge pressure sensor for each flight condition revealed differences in the data. It was found that the relative proportions of the main rotor frequency content of the leading edge pressure data varied with flight condition, thus allowing the regions shown in figure 3 to be identified. Examination of the data in the time domain using statistical techniques complemented this process. Only when specific flight conditions were selected for in-depth analysis to determine the interaction mechanisms was a revolution by revolution study of the data made. The time dependency of some aspects of the interactions made dynamic graphics a most useful tool. The animation technique employed was as discussed in Ellin⁽⁴⁾

The detailed mechanisms determined for the main rotor/tail rotor interactions will be described in the next section.

3 Interactions.

3.1 Variations in tail rotor loading distributions in hover.

Generally, the presence of a main rotor interactive effect on the tail rotor can be detected by inspection of the blade leading edge pressure sensors' signal frequency content. Analysis of the data reveals frequencies of 1R or, more commonly, 4R and their interference frequencies with the tail rotor $nT \pm 4R$. An exception to this general rule occurs in and around the hover. In these conditions, even though the main rotor wake does not cut across the tail rotor, it passes close enough to the disc leading edge to distort the tail rotor blade tip vortices nearest to the main rotor wake so that they lie outboard of the tip of the following blade. The resultant gap in the otherwise axis-symmetric ring of high $-C_p$ and thus high blade loading is shown in figure 4. Negative C_p is conventionally plotted as its increase results in a rise in blade incidence and loading. The tail rotor sensors will not be affected by any cyclical variation in the main rotor wake in this condition, hence the lack of main rotor frequencies. This interaction is discussed by Brocklehurst⁽⁸⁾ where a likely mechanism is described.

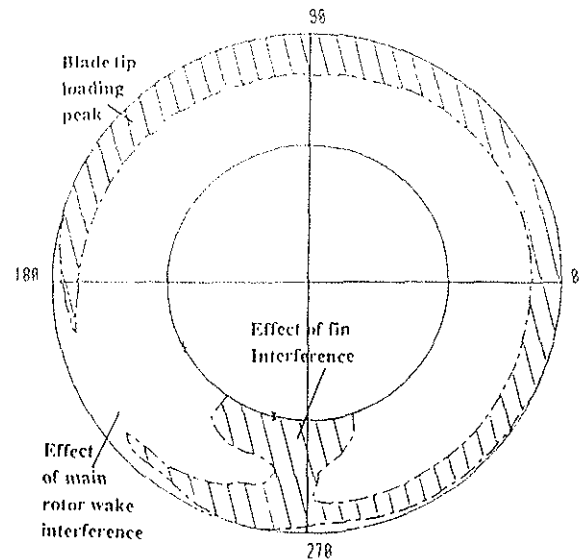


Figure 4. Locations of the regions of high $-C_p$ for one revolution of the tail rotor in an OGE hover. Localised reduction in loading is the effect of the main rotor wake.

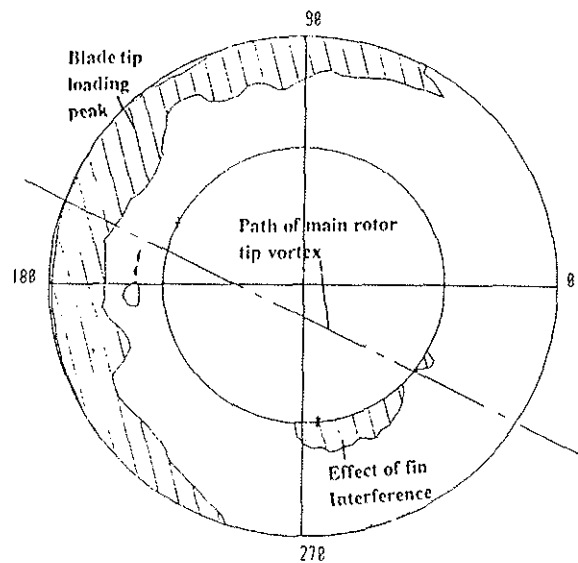


Figure 5. Location of the regions of high $-C_p$ for one revolution of the tail rotor in 30kts forward flight OGE.

3.2 Variation in tail rotor loading distribution in low speed forward flight.

When the aircraft is moving forward at low speed, the tail rotor can become partially or even totally immersed in the main rotor wake. Figure 5 is similar to figure 4 but shows the tail rotor in 30 knots

forward flight. The loading peak shown in figure 4 is missing at the rear of the disk as the trailing tail rotor blade tip vortices are left behind by the aircraft motion. The track of the successive trailing main rotor blade tip vortices is also shown; the effect of their interaction with the tail rotor changing as they cross the tail rotor disc. Outboard, within the loading peak region, the main rotor vortices cause a local reduction in the $-C_p$ value as shown at the indicated position in figure 6.

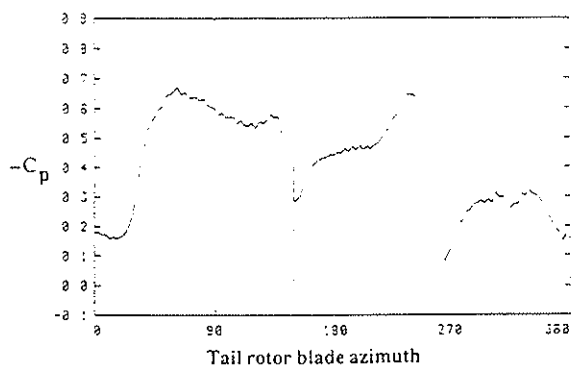


Figure 6. Variation in $-C_p$ at the 98% blade radius leading edge sensor for one revolution of the tail rotor. The localised reduction in $-C_p$ indicated by the vertical line is caused by the interaction of a main rotor blade trailing tip vortex and the preceding tail rotor blade.

Inboard the main rotor vortices cause a local peak followed by a trough in the $-C_p$ value as shown in figures 7 & 8. The trough is not always apparent.

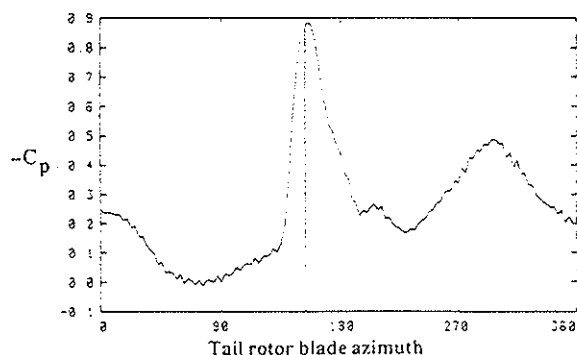


Figure 7. Variation in $-C_p$ at the 75% blade radius leading edge sensor for one revolution of the tail rotor. A main rotor vortex is approaching the sensor and the localised increase in $-C_p$ indicated by the vertical line is due to the velocity induced by that vortex opposing blade rotation.

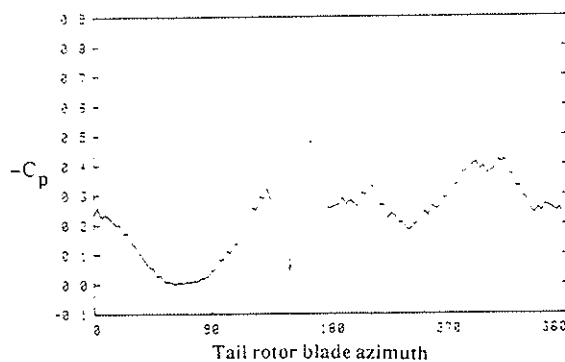


Figure 8. Variation in $-C_p$ at the 75% blade radius leading edge sensor for one revolution of the tail rotor. A main rotor vortex has just passed the sensor and the localised reduction in $-C_p$ indicated by the vertical line is due to the velocity induced by that vortex being with blade rotation.

Close examination of this interaction effect, especially with the data animated on video, has revealed a discontinuity in the timings of the passage of the effect of the main rotor vortices as shown in figure 9.

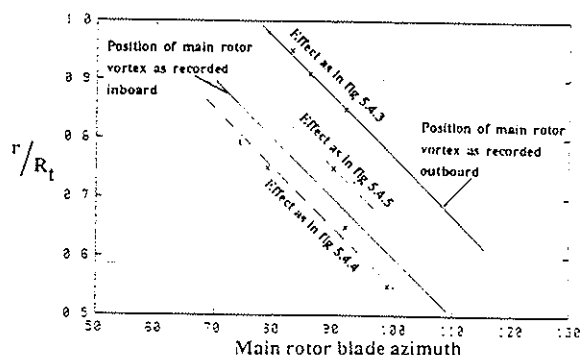


Figure 9. Plot showing the position of the datum main rotor blade as the main rotor blade trailing tip vortex interference effect is detected at each tail rotor blade leading edge sensor.

The two solid lines on the figure indicate the apparent timing of the passage of the main rotor blade trailing tip vortices. The main rotor vortices pass over the inboard tail rotor leading edge sensors midway between the passage of the peak and the trough and this is taken into account in the figure by the solid line between the 2 dotted ones. The effect of this 'phase shift' is to delay the appearance of the interactional feature in the tip loading peak region until after it has appeared further inboard. It is hypothesized that 2 different interactional mechanisms are employed, one covering the interaction between

the main rotor tip vortex and the tail rotor tip vortex and the other between the main rotor tip vortex and the tail rotor blade vortex sheet. The shift shown is approximately 15.5 degrees of main rotor rotation.

Although the two interactions described have a noticeable effect on the tail rotor C_p distribution, their overall effect on the tail rotor thrust is small. It is considered that there would be little to be gained from any attempt to reduce their effect still further. The relative magnitude of the overall tail rotor loading variation should be considered when deciding whether to include the effects of these interactions in a computer model. On a simple model of tail rotor thrust they could perhaps be ignored.

3.2.1 The interaction between a main rotor blade trailing tip vortex and a tail rotor blade trailing tip vortex in forward flight.

The interactional mechanism described in this section take place in flight conditions where the tip vortices trailed from the main rotor blades are cut by the tail rotor blades. For there to be an effect on the tail rotor loading distribution this intersection must take place when the tail rotor blade in question is at an azimuth angle where the loading peak is evident. This will limit the visible effect of this interaction to the front of the tail rotor disc.

Assuming that the wakes from the main rotor and the tail rotor were independent and that each had no effect upon the other, the blade trailing tip vortex systems from the two rotors could be drawn as skewed helices. To add complication, the shape of each element on the helices trailed from a rotor would be distorted by the wake contraction and the influence of all the other vortex elements in that rotor's wake. The relative geometry of the main rotor and tail rotor dictates that the helical wake systems from the two rotors will intermesh orthogonally. As the external influences on both wake systems are the same at any given point, the separation between a vortex trailed from a main rotor blade and one from a tail rotor blade will remain constant. The separation between a main rotor vortex element and a tail rotor vortex element will therefore be dependant on the location of that main rotor vortex element when the tail rotor vortex element was formed. A tail rotor blade trailing tip vortex is formed by the rolling up of the vortex sheet shed from the blade outboard of the point of maximum circulation. This roll up process is complete by the time that the blade tip has travelled one rotor radius (ie 60 degrees of blade rotation) (9) and the main rotor blade trailing tip vortex will have been present at it's final location whilst this roll up was taking place. The separation distance between successive main rotor and tail rotor

vortices will be different because of the non-integer gearing ratio between the two rotors.

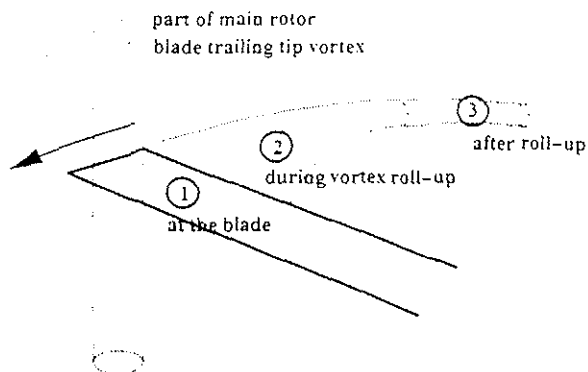


Figure 10. Sketch of main rotor blade trailing tip vortex/tail rotor blade trailing tip vortex interaction showing three phases of interaction.

Contrary to the assumption made at the beginning of the last paragraph, the two wake systems are not independent and each main rotor vortex element will induce motion in each tail rotor vortex element and vice versa. The velocities induced will depend on the strengths of the vortices and the distance between them. Figure 10 shows a sketch of the tip of a tail rotor blade with the trailing tip vortex rolling up behind it. The tail rotor blade is about to cut a main rotor blade trailing tip vortex. That main rotor vortex can induce large variations in the local chordwise velocity at the blade, possibly affecting the point of maximum circulation on the blade and thus subsequently the strength and location of the tip vortex. The vortex sheet shed by the blade may be distorted by the velocities induced by the main rotor vortex. This would affect the roll up process which would again change the properties of the tail rotor tip vortex. Once the roll up process has been completed the two vortices would continue to interact.

The overall mechanism of this interaction process is indeed complex. In an attempt to illucidate the interaction that would occur once the tail rotor blade trailing tip vortex was fully formed (and there is some doubt as to whether this would happen) a simple computer model was constructed. Two Scully vortices of approximately Lynx main and tail rotor vortex strengths were placed, one along the x-axis and the other parallel to the z-axis as shown in figure 11. The minimum separation distance between the centrelines of the two vortices was set as being the sum of the two vortex core diameters (10 cm). The vortices were initially divided up into 4mm long elements. The Biot-Savart Law was then employed to calculate the velocities induced at the core of each vortex element node by the velocity field of each vortex element from both vortices. Neglecting any inertial effects, the

displacement of each node was then calculated over a 1 millisecond timestep. This process was then repeated several times. The interaction produced was very unstable with the vortex cores touching after only four iterations and the convoluted bundle of distorted vortices growing rapidly thereafter. It was observed that the vortex elements close to the interaction were very rapidly stretched. To reduce the errors introduced by using straight vortex elements in regions of high vortex curvature, each element was kept close to its original length by cutting it in half whenever it stretched to twice its original length. This model, though simple and restrictive, illustrates the stretching of the vortex elements close to the original point of minimum separation which is considered to be significant.

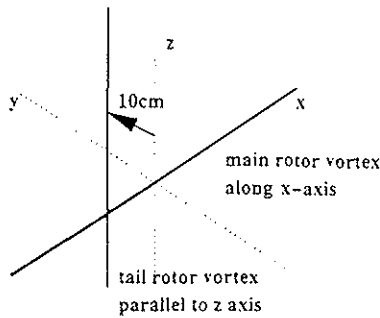


Figure 11. Vortex interaction model starting positions.

Theoretical research has been carried out by Moore & Saffman⁽¹⁰⁾ on the effect of strain on a line vortex. This suggested that a line vortex will "disintegrate" (their word) if the ratio of applied strain rate over vortex circulation strength exceeds a given value. Applying this principle to the interaction under consideration, each vortex element is subjected to a varying strain by the others. This may suggest that, when the main and tail rotor blade trailing tip vortices are close enough together, then at least the tail rotor vortex, and possibly the stronger main rotor vortex, would disintegrate and the local induced velocity field(s) fall to zero. This would have only a minimal effect on the blade trailing the vortex. However, the strength of the loading peak near the tip of a blade is most significantly affected by the location of the tip vortex trailed from the preceding blade. If that tip vortex had a discontinuity produced by the interaction just described, then a reduction in the loading peak on the next blade would follow.

For such an effect to be recorded on the instrumented tail rotor blade, the main rotor blade trailing tip vortex would have had to interact with the tip vortex trailed from the preceding tail rotor blade. This will affect the timing of the interactional feature noted in the data, effectively delaying it by 90 degrees of tail

rotor rotation. This agrees with the phase shift noted on figure 9.

The reduction in the loading peak will not be limited to the passage of one tail rotor blade. The reduction in the loading peak on one blade will reduce the strength of the tip vortex trailed behind that blade and thus affect the loading peak on the next, though to a lesser extent. Therefore, although the loading peak will be rapidly reduced by the interaction, it will return to its original value at a slower rate.

3.2.2 The interaction between a main rotor blade trailing tip vortex and the inboard region of a tail rotor blade in forward flight.

For the interaction described in section 3.2.1 to take place a main rotor blade trailing tip vortex must be cut by that part of a tail rotor blade that is outboard of the point of maximum bound circulation. If the main rotor vortex is positioned such that it will lie inboard of that point then a different interaction will occur. With the main rotor vortex far enough inboard, its distance from the tail rotor trailing tip vortex should result in there being insufficient strain on that vortex for disintegration to occur.

In low speed flight, the dominant loading variations over the region of the tail rotor blade inboard of the loading peak is caused by the change in the local chordwise velocity. This is in contrast with the dominant variations outboard being caused by changes in the inflow velocity. The inboard vortex sheet shed from a tail rotor blade does not have a particularly strong effect on the following blades. Any disruption of this shed vorticity by a main rotor blade trailing tip vortex will therefore not significantly alter the blade loading.

The axis of tail rotor rotation lies parallel to the centerlines of the main rotor blade trailing tip vortices that pass across it. Although there is some axial flow within the main rotor vortex core, it will only affect a very small part of the tail rotor disc (the core diameter being approximately 4cm) and can thus be ignored. The effects of the changes in tail rotor blade chordwise velocity induced by the main rotor vortex will vary dependant on the tail rotors direction of rotation. The vortex's velocity field will always rotate in a top-forward direction.

The lift produced by an element of the blade, dr , at radius r is given by:

$$L = \frac{1}{2} \rho V^2 dr c_a \alpha \quad \text{Eqn 1}$$

where:

$$\alpha = \theta - \tan^{-1} \frac{U}{V} \quad \text{Eqn 2}$$

giving:

$$L = \frac{1}{2} \rho c r \alpha V^2 \left(\theta - \tan^{-1} \frac{U}{V} \right) \quad \text{Eqn 3}$$

The effect of the main rotor blade trailing tip vortices on the in-plane velocity at the tail rotor blade is of a very transitory nature. For this reason, it has been assumed that the local inflow velocity, U , will not have time to change in response to the changing in-plane velocity and incidence. Therefore, when the local chordwise velocity increases not only does the V^2 term increase but the local incidence does as well. Concentrating on the V^2 term and expanding

$$V = V_r + V_v \quad \text{Eqn 4}$$

If the chordwise component of the vortex induced velocity V_v is against the direction of blade rotation, then:

$$V^2 = V_r^2 + 2V_r|V_v| + |V_v|^2 \quad \text{Eqn 5}$$

If, however, V_v is in the direction of blade rotation:

$$V^2 = V_r^2 - 2V_r|V_v| + |V_v|^2 \quad \text{Eqn 6}$$

Therefore, at a given point on the blade, the increase in blade loading that results from a vortex induced chordwise velocity opposing blade motion will be greater than that from the same velocity in the direction of blade travel. The major perturbation in blade loading will therefore be a sharp upwards peak to one side of the vortex core with a much smaller downwards one on the other. For a tail rotor with top-blade-aft rotation, such as that on the Puma of Lynx AH Mk7 the region of reduced V^2 will be on the side of the vortex centreline closer to the rotor axis. As the value of V_r is lower the further you are from the blade tip the region of reduced loading will be smaller and have less effect than would be the case with a tail rotor rotating top-blade-forward. Figures 12 and 13 show plots of V^2 against tail rotor blade radius for the 2 different blade rotations. Main rotor vortices are shown in three locations demonstrating that, for both directions of blade rotation, the effect of the vortex

decreases as it moves towards the centre of the rotor. It should be remembered that the interaction described in section 3.2.1 will mask the effect described in this section from about 80% rotor radius outwards at the front of the tail rotor disc in forward flight.

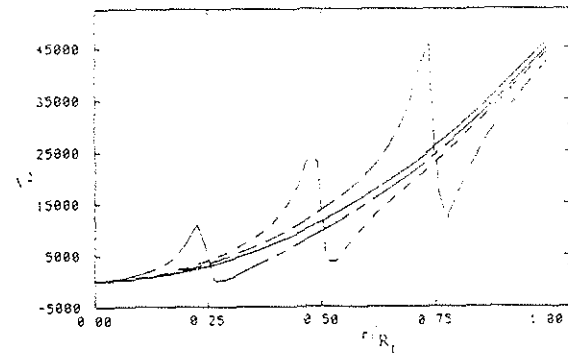


Figure 12. Theoretical variation in V^2 with blade radius for a tail rotor rotating top blade forward. The effect of a main rotor blade trailing tip vortex is shown for three vortex locations (25, 50 & 75% rotor radius).

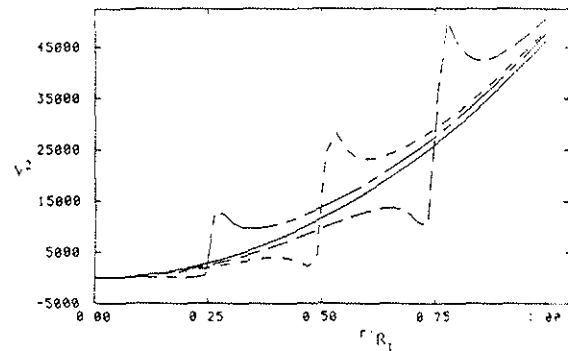


Figure 13. Theoretical variation in V^2 with blade radius for a tail rotor rotating top blade aft. The effect of a main rotor blade trailing tip vortex is shown for three vortex locations (25, 50 & 75% rotor radius).

3.3. Interaction between the main rotor wake and the tail rotor in quartering flight.

Of all the main rotor/tail rotor interactions examined in this study, that occurring in quartering flight and described in this section has the most significant effect on tail rotor performance. In this context, "quartering flight" describes the flight condition when the sideslip angle is such that the tail rotor is affected by the wake from the edge of the main rotor disc as depicted in figure 14. In forward flight the tail rotor will be in the centre of the main rotor wake and,

where they affect the tail rotor, will cut each main rotor blade trailing tip vortex in sequence as they are trailed from the rear of the disc. In quartering flight, ie with a sideslip angle of between 45 and 70 degrees depending on aircraft configuration, the main rotor wake effect on the tail rotor can be much more significant as the tail rotor may be immersed of one of the two 'wingtip' vortices trailed from the edges of the main rotor disc. The distortion of the main rotor wake caused by the formation of these wingtip vortices is well documented by Heyson & Katzoff(11) and Brocklehurst(8).

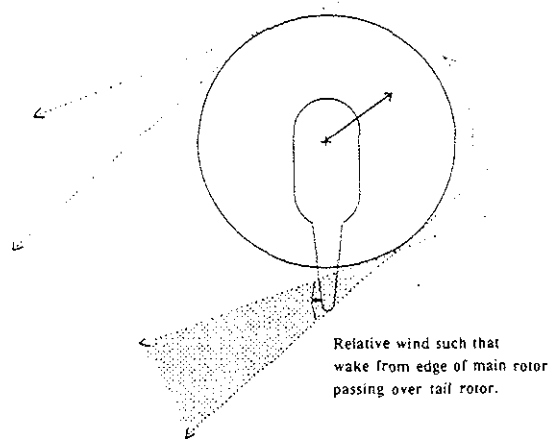


Figure 14. Definition of quartering flight.

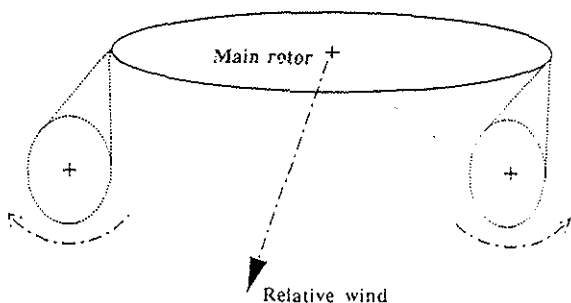


Figure 15. Direction of rotation of both "wing-tip" vortices is bottom-away from aircraft centreline.

The wingtip vortex is formed from a number of main rotor blade trailing tip vortices rotating round each other. In forward flight the velocity field of each of these trailing vortices will also be rotating such that motion below the vortex centreline will be directed outwards, away from the aircraft centreline as shown in figure 15. The wingtip vortex will therefore constitute a significant velocity field, all rotating in

this direction. Once the aircraft develops a sideslip angle the wingtip vortices maintain their position with respect to the aircraft's track which will no longer be aligned with the axis of the helicopter. As just mentioned above, with a sideslip angle of 45 to 70 degrees the helicopter's tail rotor may end up tracking along one of these vortices. If the tail rotor rotates top-blade-forward and the centre of the wingtip vortex passes through the centre of the tail rotor disc as in figure 16, then the tail rotor blades will be rotating within a mass of air that already has a component moving in the same direction. The flow velocity over the blades will therefore be reduced. The resultant reduction in dynamic head means that an increased tail rotor blade pitch is required to produce the necessary thrust. This increased pitch requirement is reflected in the helicopter transmission and control system by a reduction in pedal margin. The situation is the same whether the tail rotor is affected by the wingtip vortex from either the advancing or the retreating side of the main rotor disc (areas 3 & 4 on figure 3). The only difference that exists between the two is that when the tail rotor is affected by the vortex from the retreating side of the main rotor, the tail rotor is off-loaded to some extent by the weathercocking action of the fuselage and the change in tail rotor inflow due to the sideways motion. The yaw control margin is therefore greater than with the same relative wind from the other side of the nose and its reduction proportionally smaller.

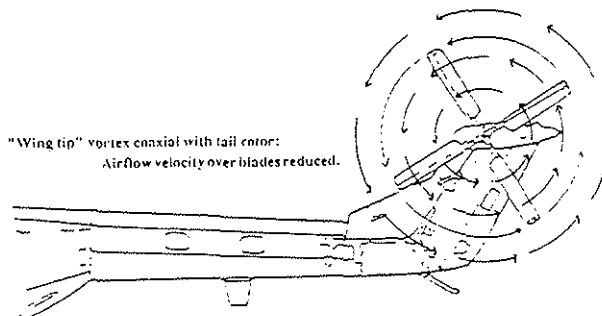


Figure 16. "Wing-tip" vortex coincident with tail rotor.

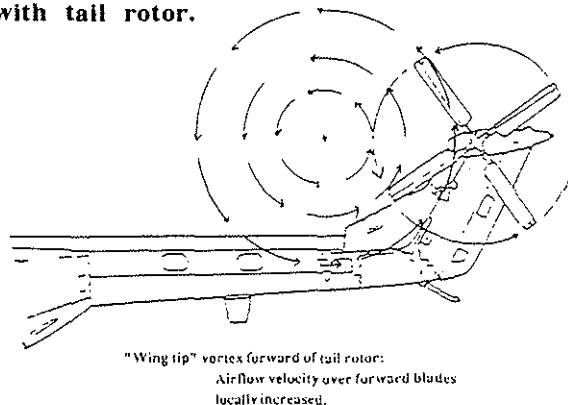


Figure 17. "Wing-tip" vortex forward of tail rotor.

When the centre of the tail rotor disc is displaced from the vortex centreline as depicted in figure 17, that part of the tail rotor disc between the vortex centreline and the axis of rotor rotation will experience an increase in dynamic head. As shown in figure 18 the effect of a vortex tracking diametrically across the tail rotor will be an initial rise in dynamic head followed by a much larger fall before a mirror image effect on the other side of the disc. The strength of the vortex used in this figure is not representative of that behind a Lynx main rotor but merely illustrative to show the effect.

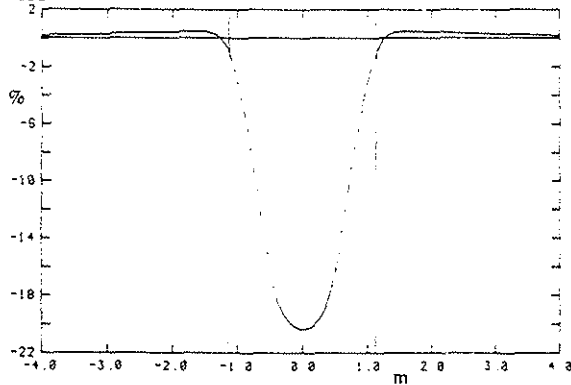


Figure 18. Percentage change in overall tail rotor dynamic head as a representative "wing-tip" vortex tracks diametrically across the disc. Tail rotor radius is 1.1m.

With a tail rotor that rotates top-blade-aft the effect of the wingtip vortex on the yaw control margin is reversed.

It could be expected that the tail rotor would be closer to the start than the end of the wingtip vortex roll up process. The velocity fields round the main rotor vortices would therefore show a marked cyclical variation at the blade passing frequency which would be detected at the tail rotor pressure sensors. Even if the roll up was well established this frequency would still be evident if the rolled up vortices retained their identities. As the effect of the main rotor wake on the tail rotor is stronger in this flight condition than in forward flight it would be reasonable to expect that the main rotor induced frequency content would be stronger too. This has not been found to be the case; in fact the tail rotor blade pressure sensors display a distinct lack of main rotor frequency content in the areas of the flight envelope where the pedal margin was reduced. This would suggest that the individual main rotor blade vortex cores had merged into one single larger core whose associated velocity field would display a significantly reduced cyclical content. This vortex merging had been noted during research carried out into wake minimisation techniques for large transport aircraft by Rossow⁽¹²⁾. In that reference it was found that the major criterion determining

whether the two vortex cores merged or not was the ratio of the distance between their centrelines and the cores' diameter. If merging of this nature has occurred it would suggest that the roll up process was approaching completion. The relative strength of the flow field round the merged vortex compared with its individual elements requires further investigation as does its longevity.

With the intention of showing whether this merging was indeed a cause of the reduction in main rotor frequencies, it was decided to construct a Lynx main rotor wake model and examine the vortex separation at different forward flight speeds. The model eventually selected as being the most accurate available that would run at a reasonable speed was that described by Beddoes⁽¹³⁾.

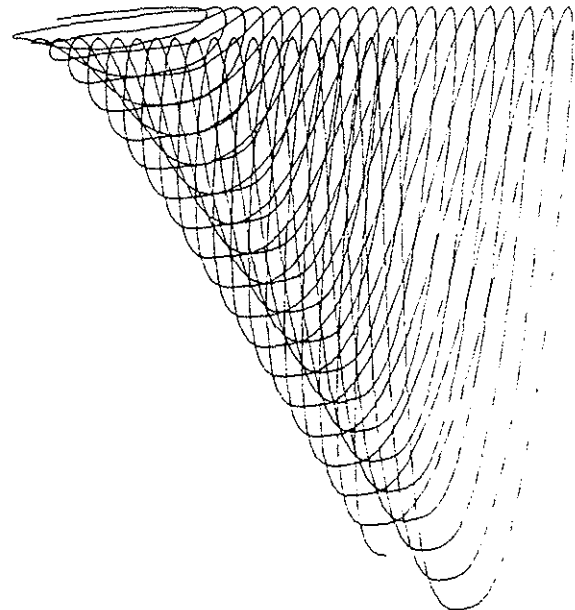


Figure 19. Beddoes main rotor wake model configured as a Lynx at 30 knots.

The model is of a prescribed wake that reflects the wake distortions observed by Heyson. The wake model was coded up without deviation from the algorithms in the paper and run with parameters selected to represent a Lynx under the same loading as the trial data (figure 19). On examination of the vortex placement it was found that the separation ratio described above predicted that vortex merging could occur at the flight conditions of interest (figure 20).

Encouraged by this result it was decided to investigate more fully the model's potential. It was reconfigured to show the number of main rotor vortices passing through the tail rotor disk at a range of flight conditions within the low speed envelope. Displayed on a polar plot (figure 21), this data showed more than a passing resemblance

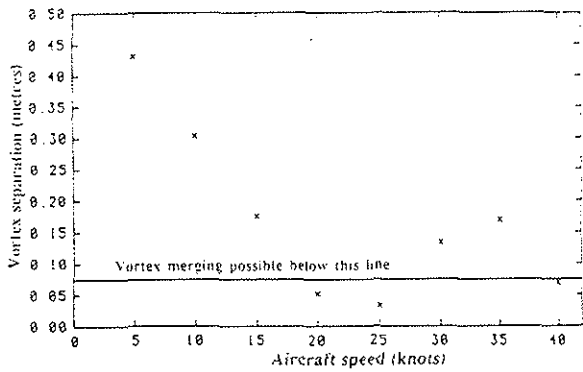


Figure 20. Variation in minimum separation distance between individual blade trailing tip vortices within the "wing-tip" vortices with aircraft speed as calculated for a Lynx AH Mk5.

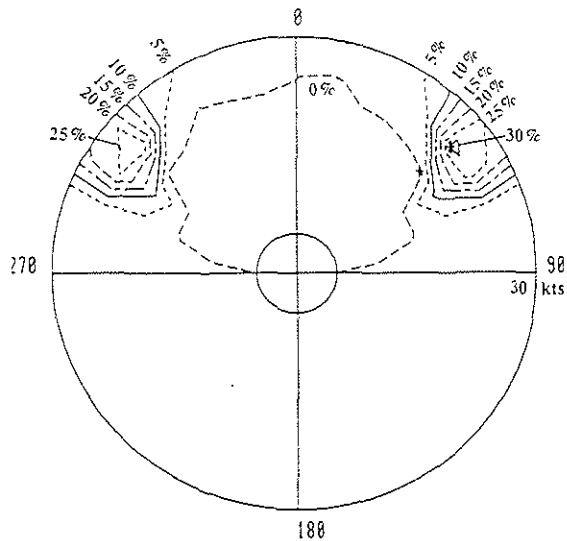


Figure 22. Variation in total tail rotor dynamic head as calculated using Helistab in conjunction with the Beddoes main rotor wake model.

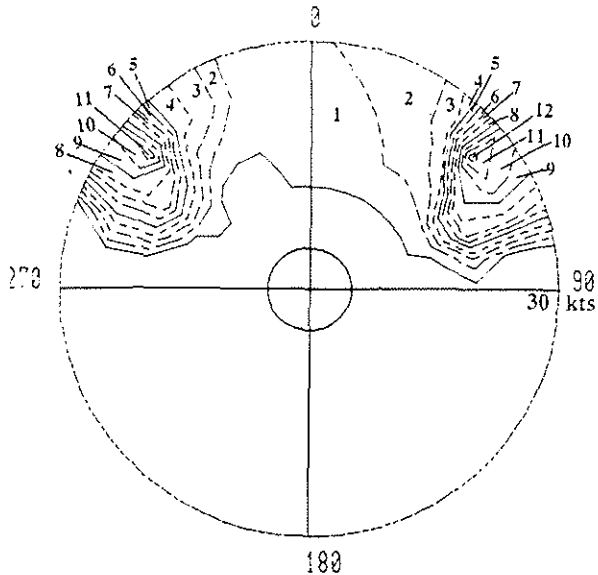


Figure 21. Variation in number of main rotor blade trailing tip vortices passing through the tail rotor with flight condition as calculated using the Beddoes wake model.

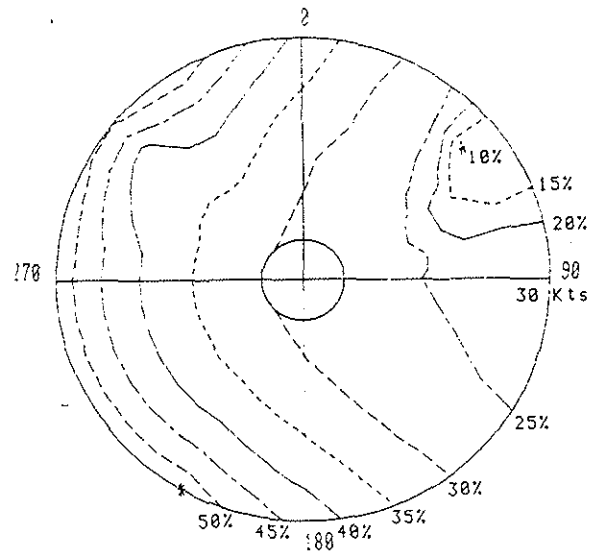


Figure 23. Variation in pedal margin with flight condition as calculated using data from figure 22.

to the plot of pedal margin. To investigate the extent of the relationship between these 2 parameters the model was extended by inclusion of a model of a Scully vortex velocity distribution as described by Beddoes (13). It was then used to calculate the component of the velocity induced by the main rotor vortices parallel to the tail rotor blade chord. From this a percentage reduction of dynamic head at the tail rotor was calculated. Again, as expected, a similar pattern emerged (figure 22). This reduction in dynamic head necessitates a proportional increase in tail rotor root pitch angle if the rotor is to produce the same thrust. The results obtained from Helistab were modified to include this effect and the resultant plot of yaw pedal margin against flight condition is shown in figure 23.

Calculation of the reduction in dynamic head is a lengthy and expensive process. The velocities induced by each element of the main rotor wake at each point on the tail rotor must be calculated unless some method is used to determine those wake elements having the most significant effect. In an attempt to arrive at the same value of root pitch by a significantly faster route, the value for percentage dynamic head reduction was replaced by a suitably factored value of the number of main rotor vortices taken from figure 21. The resultant value of dynamic head reduction is shown in figure 24 which,

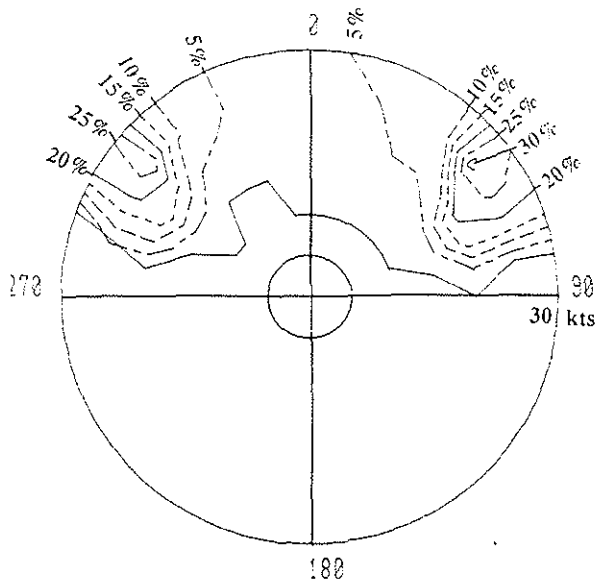


Figure 24. Reduction in tail rotor dynamic head calculated using data from figure 21.

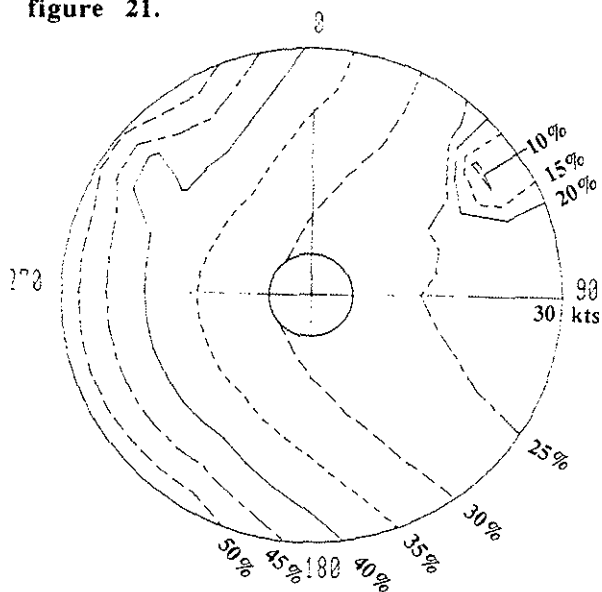


Figure 25. Variation in pedal margin with flight condition as calculated using data from figure 24. Compare with figure 2.

except in minor detail, is comparable with that in figure 22. Converting this into a pedal margin (figure 24) and comparing with the flight measured values (figure 2), it can be seen that, by applying a simple correction factor to the blade angle calculated, we have achieved a significant improvement to the pedal trim position over that originally given by the model.

It is appreciated that various approximations and assumptions have been made in achieving this result. The main rotor wake is a prescribed model and does

not reproduce accurately the vortices at the edge of the wake. In addition, no account is taken of any distortion of the main rotor wake by the tail rotor. The fine details of the vortices rolling round each other and any vortex merging that occur are not included. The exact location of the vortices from which the reduction in dynamic head is calculated will not be precise, but it is assumed that, so long as the figure used is for an overall reduction over the entire tail rotor disc, the result achieved will be reasonably accurate. The tail rotor in Helistab is represented by a disc model, so the requirement is for a factor that can be applied to the rotor as a whole rather than to individual blade elements. It would not be reasonable to expect the model to produce accurate values of local incidence as these would be very dependent on vortex position. For this reason no correction for changes in incidence have been included in the calculation even though they would affect the outcome. The velocities induced by the main rotor vortex sheet will also affect the tail rotor loading. This effect is to be studied in due course. No attempt has been made to include fin interference effects as the data on this have yet to be analysed. The magnitude of the fin interference will vary dependent on the location of the main rotor wake (see Brocklehurst⁽⁸⁾) and will thus introduce a non linear variation into the pedal margin plot. Notwithstanding the above, it is considered that the predominant effect on the pedal margin is the dynamic head reduction caused by the main rotor tip vortex and that the approach taken is justified.

As far as use of this pedal margin improvement in helicopter simulation is concerned two possible approaches are envisaged. The first would be to take the dynamic head reduction and apply it to the tail rotor blade root pitch angle via a look-up table. This would be the simplest to embody but of questionable accuracy. The wake model is of steady level flight and thus the correction factor used would assume that the model had been at its current speed/sideslip combination in level flight for a number of main rotor revolutions. The preferred option would be to convert the main rotor wake model to a manoeuvre wake model which responded directly to the aircraft motion. This model could then be used to calculate the number of main rotor vortices passing through the tail rotor and a correction factor derived. It is believed that a more accurate pedal margin would be achieved by this method though this does require substantiation. The manoeuvre wake model would need to run in parallel with the aircraft model and to run in real time.

3.4 Main rotor frequency content on tail rotor signals in rearward flight.

In flight with a rearward component of aircraft translational velocity OGE the tail rotor cannot be immersed in the main rotor wake. The same is not the case for flight IGE where the roll up of the ground vortex will have a significant effect on the tail rotor performance (see Weisner & Kohler⁽¹⁴⁾) It was therefore surprising to find significant main rotor frequencies in the Lynx tail rotor pressure data. Two different forms of this interaction were found, one in figure 6 region 5 where the main rotor blade passing frequency, $4R$, was dominant and the other in region 6 where the main rotor rotational frequency, R , took its place. Although other mechanisms such as acoustic feedback and the interaction of the main rotor blades with the tail rotor far wake were considered, the most likely cause of this effect was considered to be the main rotor forcing the fuselage which, in turn, caused the tail rotor blades to flap giving rise to small changes in loading. The fact that all 7 sensors along the length of the blade appear to be equally affected would tend to rule out a direct aerodynamic interaction which would affect one part of the blade more than the remainder. The effect of this interaction would be to impart a small additional yawing moment to the fuselage in the same direction as the movement of the tail, be it yaw or sway, that gave the input to the tail rotor.

4. Conclusions and recommendations.

A series of flight trials has been conducted with the DRA's flight research helicopter to provide a better understanding of the effects influencing tail rotor performance and yaw control. From the data analysis carried out to date the following conclusions can be drawn:

1. Six distinct mechanisms of main rotor/tail rotor interaction have been noted in the low speed envelope, the most significant of which have been examined in detail.
2. In quartering flight, the tail rotor can be immersed in the roll-up of the main rotor blade tip vortices trailed behind the edge of the disk. For a tail rotor rotating top-blade-forward, this results in a large net reduction in the dynamic head at the blade giving rise to a reduction in control margin. This is the most significant interaction influencing the tail rotor and its effect should be included in any helicopter model.
3. This interaction can be adequately modelled using a simple prescribed main rotor wake

representation giving the potential for improved accuracy in simulator pedal margin.

4. Close to the hover, the main rotor wake passes just forward of the leading edge of the tail rotor disc distorting the tail rotor trailing vortex wake. This results in a localised reduction in tail rotor loading.
5. In low speed forward flight the main rotor blade tip vortices can interact with the tail rotor tip vortices and, where the distance between the two vortices is small, they each impose a strain field on the other which can cause vortex disintegration with a resultant reduction on the tip loading peak on the following tail rotor blade.
6. In low speed forward flight the main rotor blade tip vortex can interact with the section of the tail rotor blade inboard of the lading peak producing changes in the local chordwise velocity and incidence at the blade with consequent variations in blade loading.
7. In rearwards flight the tail rotor can experience small loading variations at main rotor induced frequencies possibly due to main rotor wake effects on the fuselage causing sideways movement of the tail rotor gearbox and hub.

The furtherance of this study would benefit from the following additional investigations:

- i. An experimental investigation of orthogonal vortex interaction to study the detail of main rotor blade tip vortex/tail rotor blade tip vortex interaction.
- ii. An experimental investigation of blade vortex interaction with the vortex perpendicular to the blade surface.
- iii. A flight trial with an instrumented tail rotor with sensors that would permit the calculation of the local chordwise velocity. A feasibility study is currently being undertaken for a trial with an instrumented rotor on the the DRA flight research Lynx AH Mk7 helicopter. The aircraft would also be fitted with a tail rotor torque meter and a load cell to directly measure tail rotor thrust. As the significant difference between the Lynx Mk5 and Mk7 is the direction of tail rotor rotation, a comparison of the data sets from the proposed trial and the one already conducted would yield much information on the detail of the effects of tail rotor direction of rotation, particularly in quartering flight.
- iv. Further study on the implementation of main rotor wake effects in simulation models to improve the quality of yaw axis response. The approach described has only been tried for a Lynx AH

Mk5. Its general applicability has still to be determined.

v. More in-depth analysis of the data collected in the tail rotor trials to date to look in detail at the effects of interaction with the fin and the ground, and to look at the causes, detection and effects of tail rotor blade stall.

References.

- 1 Padfield,G.D. A theoretical model of helicopter flight mechanics for application to piloted simulation. RAE Technical Report 81048, 1981
- 2 Baldwin,S.F. and Handley,C.S. Flight tests to explore tail rotor limitations in the low speed envelope. 14th European Rotorcraft Forum, Milan, 1988, paper 111.
- 3 Ellin,A.D.S. and Brown,C.D. RAE Bedford tail rotor aerodynamic flight research programme - Lynx AH Mk5 trial conduct. SEFTE Conference on Helicopter Flight Test Techniques, Patuxent River, 1991.
- 4 Ellin,A.D.S. Flight measurements illustrating key features of tail rotor loading distribution. Royal Aeronautical Society Conference on Helicopter Yaw Control Concepts, London, 1990.
- 5 Ellin,A.D.S. Tail rotor aerodynamic features recorded in flight. 16th European Rotorcraft Forum, Glasgow, 1990, paper I.4.4.
- 6 Brotherhood,P. and Riley,M.J. Flight experiments on aerodynamic features affecting helicopter blade design. Vertica, 1978, Vol 2, pp27-42.
- 7 Brotherhood,P The determination of helicopter blade local normal force coefficient, incidence and stall boundaries from flight measurements of leading and trailing edge pressures. DRA Technical Memorandum in preparation, 1992
- 8 Brocklehurst,A. Main rotor/tail rotor interactions near hover. Westlands RM 535, 1986. Not in public domain.
- 9 Simons,I.A., Pacifico,R.E. and Jones,J.P. The movement, structure and breakdown of trailing vortices from a rotor blade. A.R.C.28 993, 1967.
- 10 Moore,D.W. and Saffman,P.G. Structure of a line vortex in an imposed strain. Proceedings of Symposium on Aircraft wake turbulence and it's detection, 1970, pp339-354.
- 11 Heyson,H.H. and Katzoff,S. Induced velocities near a lifting rotor with nonuniform disk loading. NACA report 1319, 1957.
- 12 Rossow,V.J. Convective merging of vortex cores in lift-generated wakes. Journal of Aircraft, 1977 Vol 14, No.3, pp283-290.
- 13 Beddoes,T.S. A wake model for high resolution airloads. Proceedings of US Army/American Helicopter Society Conference on Rotorcraft Basic Research, Maryland,1985.
- 14 Wiesner,W. and Kohler,G. Tail rotor performance in the presence of main rotor, ground, and winds. Journal of the American Helicopter Society, 1974, Vol 19, No.3.

© British Crown Copyright 1993 /DRA

Published with the permission of the Controller of Her Britannic Majesty's Stationery Office.

The research reported in this paper was conducted as part of the UK MoD Strategic Research Programme (item AS011Q09).